Droplet Size Distribution Effects on Aircraft Ice Accretion

R. John Hansman Jr.*
Massachusetts Institute of Technology, Cambridge, Massachusetts

The impinging mass flux distribution which determines aircraft ice accretion rate is shown to be related to the atmospheric droplet size distribution through the droplet collection efficiency of the body. Collection efficiency is studied by means of a two-dimensional droplet trajectory code which includes the effect of nonspherical droplet shape due to hydrodynamic deformation. The simulation was found to agree with wind tunnel photographic studies of droplet kinematics. The results of the simulation are used to generate impinging mass flux distributions for typical cloud and precipitation size distributions. The impinging mass approach is also used to determine relative icing rates from several supercooled cloud characterizations including the intermittent maximum icing envelope of Federal Aviation Regulation, Part 25.

Nomenclature

A = droplet area perpendicular to the relative wind
a = droplet acceleration vector
C_d = drag coefficient
D_{eq} = diameter of equivolumetric sphere
D_0 = median volume diameter
f = droplet size distribution function
H = height of body
h = height of impingement window
K_a = constant in droplet equation of motion
LWC = liquid water content
M_d = droplet mass
Re = Reynolds number based on D_{eq}
U = freestream velocity
u = fluid velocity
v = droplet velocity
v_{rel} = relative wind velocity
η = structure collection efficiency
μ = dynamic viscosity of air
ρ_a = air density
ρ_ℓ = droplet density
ϕ = impinging mass flux distribution function

Introduction

MUCH of the basic experimental and analytical icing work in the U.S. was done in the 1940's and 1950's by NACA and the aviation industry.[1,2] In the 1980's icing has re-emerged as an important area. This is due to the developing needs of the helicopter, general-aviation, and commerical-aviation communities coupled with technical advances such as high-speed digital computation.[3] The advances in computational power are extremely well suited to the calculation of droplet impingement trajectories, which are a cornerstone of any icing analysis work. Recently, several droplet trajectory codes have been written which iteratively solve the droplet equations of motion;[4-6] however, there has been very little direct experimental validation of these codes.

Presented as Paper 84-0108 at the AIAA 22nd Aerospace Sciences Meeting, Reno, Nev., Jan. 9-12, 1984; received Oct. 24, 1984; revision received March 26, 1985.

*Assistant Professor, Department of Aeronautics and Astronautics. Member AIAA.

In the following, a simple two-dimensional droplet trajectory code was developed and subjected to experimental verification. The code follows the standard approach of Langmuir and Blodgett[7] where the droplet is driven by the hydrodynamic drag. It was found that the hard sphere drag coefficients employed by most investigators do not agree with experimental results for large drops due primarily to droplet flattening. A new set of empirically corrected drag coefficients was generated from well accepted droplet terminal velocity data.[8] With the modified drag coefficients, the code was found to agree well with wind tunnel photographic studies of droplet kinematics.

The droplet trajectory code was used to study the effect of droplet size on collection efficiency. Large droplets are seen to be more important in the icing process due to their increased collection efficiency and higher mass. This size effect is quantified by the impinging mass flux distribution function which is the atmospheric size distribution function weighted by droplet mass and collection efficiency. Icing rate can be directly related to the impinging mass distribution. Using the simulation results as a guide to the collection efficiency, impinging mass flux distribution functions were generated for typical cloud and precipitation distribution functions. In addition, collection efficiency weighting was applied to the intermittent maximum icing envelope of Federal Aviation Regulation (FAR) Part 25[9] and the recent characterization of supercooled clouds below 10,000 ft.[10] The resulting relative icing rates highlight critical areas for concentration in icing certification programs.

Computer Simulation of Droplet Trajectories

A computer code to calculate droplet trajectories in an arbitrary two-dimensional flowfield has been written and is described in this section.

Droplet Equations of Motion

The equation of motion for a droplet driven by another fluid can be written from the hydrodynamic drag equation as

$$M_d \boldsymbol{a} = (C_d/2)\rho_a A |\boldsymbol{u} - \boldsymbol{v}| (\boldsymbol{u} - \boldsymbol{v}) \tag{1}$$

where $\boldsymbol{a}$ and $\boldsymbol{v}$ are the acceleration and velocity vectors of the drop, $\boldsymbol{u}$ the velocity vector of the fluid, M_d the mass of the drop, ρ_a and ρ_ℓ the densities of air and water, A the area of the drop perpendicular to the relative wind, and C_d the drag coefficient of the drop.

In order to simplify the use of Eq. (1), it is assumed that the area A of the droplet is the value for an equivolumetric sphere and that any deviation from sphericity will be included in the drag coefficient C_d. The Reynolds number for the droplets is defined as

$$Re = (\rho_a/\mu) D_{eq} v_{rel} \tag{2}$$

where v_{rel} is the magnitude of the relative wind felt by the drop and D_{eq} the equivolumetric sphere diameter.

$$v_{rel} = |u - v| \tag{3}$$

The equation of motion [Eq. (2)] now can be written in simplified form as

$$a = \left(\frac{C_d Re}{24}\right) \frac{1}{K_a} (u - v) \tag{4}$$

where

$$K_a = \frac{1}{18} \frac{\rho_\ell}{\mu} D_{eq}^2 \tag{5}$$

which is constant over a particular trajectory.

Equation (4) is the equation of motion used in the trajectory code. It has a form similar to the equation of motion first proposed by Langmuir and Blodgett.[7] The coefficient (C_dRe/24) is presumed to be a function of the Reynolds number and is discussed in a later section; K_a is constant (assuming D_{eq} remains constant); and $(u - v)$ is the relative wind felt by the droplets.

Iteration Algorithm

A flow diagram for the iterative computation of two-dimensional droplet trajectories is shown in Fig. 1. Three groups of input parameters are required: the flowfield, the initial droplet conditions, and the atmospheric conditions. The code calculates trajectories for an arbitrary, known two-dimensional flowfield. The velocity field must be input either through flow equations or by means of tabulated values. If trajectories near the bodies are being calculated, then the position of the body surfaces must be included.

The code also checks for instability which may cause large droplets to break up when experiencing high accelerations. Secondary forces such as gravity can be included also.

Drag Coefficients

In most calculations of droplet trajectories, investigators have used the drag coefficients for solid spheres[4-6] first suggested by Langmuir and Blodgett.[7]

In order to check the validity of the Langmuir and Blodgett drag coefficients C_d or, equivalently, ($C_d Re/24$), the code was used to compute the terminal fall velocity of drops in the Earth's gravitational field. The results are shown in Fig. 2, along with the well-accepted experimental results of Gunn and Kinzer.[8] The Langmuir and Blodgett coefficients predict a higher terminal velocity than observed experimentally. The reason for the discrepancy is that the Langmuir and Blodgett coefficients neglect such effects as drop deformation and the increased drag due to turbulent eddies downstream of the drop. These effects increase C_d and, hence, reduce the terminal velocity.

In order to improve on the Langmuir and Blodgett coefficients, it was decided to invert the Gunn and Kinzer experimental results to determine a set of empirically modified drag coefficients. The modified values of ($C_d Re/24$) are plotted against Reynolds number in Fig. 3, along with the Langmuir and Blodgett values. The experimental values cut off at $Re = 3500$, due to drop breakup. It is assumed that the values of ($C_d Re/24$) can be extrapolated to higher Reynolds numbers. Therefore, from Fig. 3,

$$\frac{C_d Re}{24} = 1.699 \times 10^{-5} (Re)^{1.92} \quad Re > 3500 \tag{6}$$

Using the modified drag coefficients, the terminal velocity was calculated both by code and analysis. As expected, the values agree well with the Gunn and Kinzer data for the atmospheric conditions of 1080/millibars and 20°C at which the experiments were performed.

Wind Tunnel Validation of Computer Trajectories

In order to verify the computer-predicted trajectories, droplets were observed in the setup shown in Fig. 4. Droplets were injected into a free-flowing wind tunnel perpendicular to the flow. Droplet velocity components along the tunnel axis were measured 125 cm downstream of the injection site. The measurements were made using a double strobe photographic technique. Two strobes, sequentially fired at a fixed time interval, illuminated the droplets from behind, forming a dual-image shadowgraph from which droplet velocities could be obtained.

In the initial experiment, droplets were injected into a uniform flow. The observed droplet velocities for three values of the tunnel freestream velocity (45, 60, and 75 mph) are shown in Fig. 5 along with the computer-calculated values. There is good agreement over the observed 0.15 to 1.0 mm range of equivalent droplet diameters. At the observation site, the small droplets, due to their low inertia, are close to the freestream velocity, while the larger droplets are slower and still accelerating. The minor scatter between observed and predicted values of velocity is attributed to difficulty in measuring D_{eq}, slight variations in the tunnel velocity, and perturbed initial conditions due to droplet breakup or other injection effects.

In order to confirm that the computer code predicted the trajectories in regions of spatially varying flow accurately, observations of droplet velocity were made just upstream of a cylinder. A cylinder was chosen because the two-dimensional flow ahead of a cylinder has a well-known, simple analytical form.

Trajectories ahead of two cylinders of 11.25 and 2.4 cm in diameter were observed in the wind tunnel at freestream velocities from 45 to 75 mph. Several hundred droplet velocities were observed and compared to the computed values. The measured and computed drop velocities were found to agree with a standard deviation of less than 3% of the predicted velocity for accurately photographed droplets.

In conclusion, the experimental evidence supports the results of the computer simulations. Therefore, the code can be applied to other situations of interest with some confidence in the results.

Impinging Mass Flux Distribution

In studies of aircraft icing, the primary atmospheric parameters are temperature and liquid water content (LWC). The atmospheric droplet size distribution function $f(D_{eq})$ which characterizes the spectrum of droplet size in terms of the equivolumetric sphere diameter D_{eq} is also considered an important parameter. It is essential to recognize that it is not the ambient distribution of supercooled water droplets in the atmosphere which influences the rate of ice accretion on an aircraft structure, but, rather, the mass flux distribution of droplets which actually impinge on the structure.

The impinging mass flux distribution function per unit span $\phi(D_{eq})$ can be related to the atmospheric size distribution function $f(D_{eq})$ by

$$\phi(D_{eq}) = UH \frac{4}{3} \pi \rho_\ell \left[\frac{D_{eq}}{2}\right]^3 \eta(D_{eq}) f(D_{eq}) \tag{7}$$

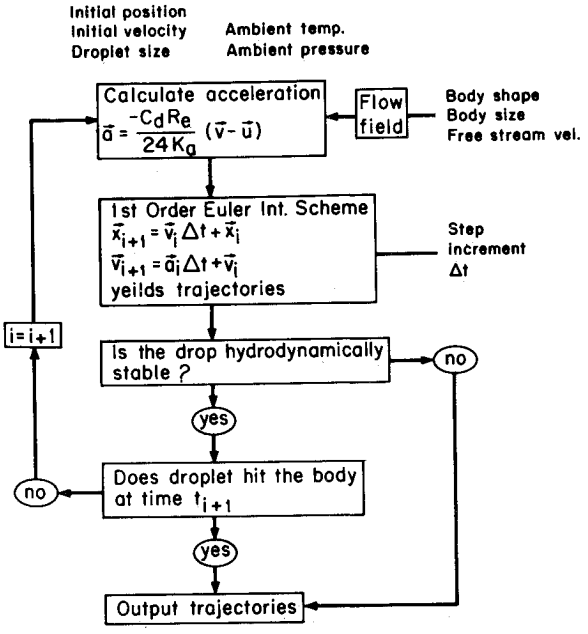

Fig. 1 Flow diagram for the trajectory code.

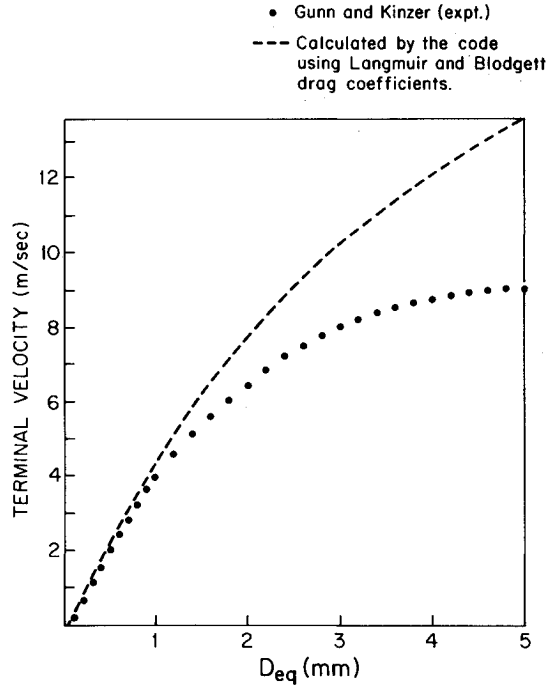

Fig. 2 Terminal velocity of water drops vs equivalent diameter.

where U is the freestream velocity, H the thickness of the structure, ρ_ℓ the density of the droplets, and $\eta(D_{eq})$ the collection efficiency of the structure, dependent on D_{eq}. From Eq. (7) it is clear that the impinging mass distribution function is significantly different from the droplet size distribution function due to the size dependence of the collection efficiency and the D_{eq}^3 volume term. The rate of ice accumulation can be obtained by integrating $\phi(D_{eq})$ over all droplet sizes.

In order to study the impinging mass flux distribution for different atmospheric cases, the previously discussed droplet trajectory simulation was employed to investigate the dependence of the collection efficiency on D_{eq}. Using the simulation results as a guide for $\eta(D_{eq})$, the impinging mass flux distribution functions are then generated for typical cloud and precipitation distribution functions.

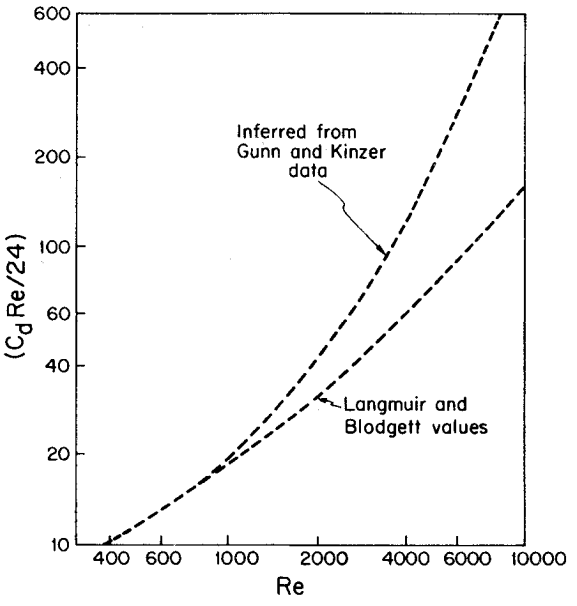

Fig. 3 Drag coefficient vs Reynolds number.

Droplet Collection Efficiency of a Half-Body

In Fig. 6, two-dimensional trajectories are plotted near a half-body for droplets of various equivalent diameters. The effect of droplet inertia is apparent—small droplets are swept by the airfoil, while the inertia of the large drops causes them to resist change in direction and they impact the airfoil. In the example in Fig. 6, the freestream velocity was 60 m/s to the left and the body thickness was 20 cm. The atmospheric conditions were typical icing values of 750 millibars pressure (equivalent altitude approximately 10,000 ft), −10°C temperature, and gravitational acceleration was neglected.

In the simulated trajectories and Refs. 11-14 it was observed that for a given droplet size only those droplets within a narrow "impingement window" around the stagnation streamline impact the body. If $h(D_{eq})$ is defined as the height of the impingement window, then it is possible to write the collection efficiency as

$$\eta(D_{eq}) = \frac{h(D_{eq})}{H} \tag{8}$$

In Fig. 7, the impingement window height is plotted against D_{eq} for a 20-cm-thick half-body simulation. The freestream velocities studied were 40, 60, and 80 m/s. It is interesting to note that droplets with D_{eq} less than 10 μm are always swept by the half-body at these velocities. Above 10 μm, the height of the impingement window increases roughly linearly with diameter up to 75 μm after which the impingement window begins to approach an asymptotic value of 10 cm. This linear behavior was also observed by Brun et al.[12,13] and Bergeron[14] in their simulations. The slight irregularities in the curves are not physical. They are a remnant of the discrete nature of the sampling algorithm and, therefore, should be ignored.

Typical Distribution

Using the preceding results as a guide for estimating the collection efficiency, it is instructive to look at the impinging mass flux distribution functions for typical cloud and precipitation size distributions.

Typical Cloud Distributions

An approximate form of the cloud size distribution function is the Khrgian-Mazan distribution[15]:

$$f_{KM}(D_{eq}) = \text{const} D_{eq}^2 \exp\{-3D_{eq}/\overline{D_{eq}}\} \tag{9}$$

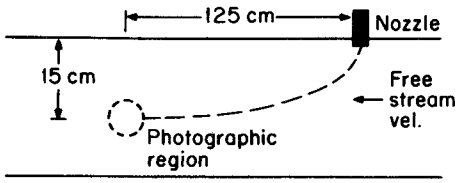

Fig. 4 Experimental setup for droplet velocity measurements.

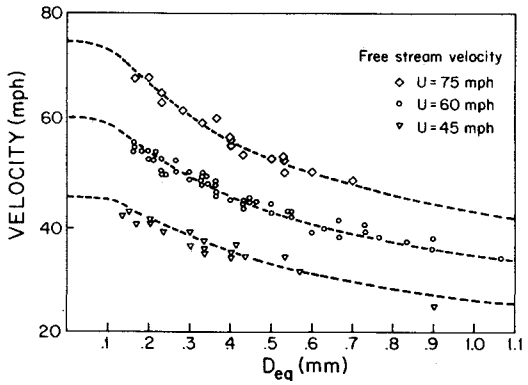

Fig. 5 Droplet velocity along the tunnel axis at the photographic region vs equivalent diameter (several values of freestream velocity).

where $\overline{D_{eq}}$ is the mean effective droplet diameter. Combining Eqs. (7-9) and noting that η is roughly proportional to D_{eq} for cloud-size droplets (10-40 μm) yields

$$\phi_{KM}(D_{eq}) = \text{const} D_{eq}^6 \exp\{-3D_{eq}/\overline{D_{eq}}\} \quad (10)$$

An example of the Khrgian-Mazan distribution function and the impinging mass distribution function is shown in Fig. 8 for $\overline{D_{eq}} = 20$ μm. It is interesting to note that the peak value of the mass distribution function occurs at 40 μm, which is twice the mean diameter $\overline{D_{eq}}$ in the cloud. Indeed, the extreme value condition for Eq. (10) yields

$$D_{eq}|\max \phi_{KM} = 2\overline{D_{eq}} \quad (11)$$

From Fig. 8 it is clear that the shape of the ambient size distribution is a very important factor in determining the icing severity of a particular cloud. A relatively low cloud liquid water content is a significant icing threat if it consists of large droplets. On the other hand, if the cloud consists of small droplets, even very high liquid water content would only cause trace icing. The strong influence that the atmospheric droplet size distribution has on aircraft icing and the lack of real-time information on the distribution make accurate forecasting of icing conditions difficult.

Typical Freezing Rain Distribution

For raindrops, the collection efficiency is approximately unity. The accepted size distribution function for rain is the Marshall-Palmer distribution,[16] further refined by Atlas.[17]

$$f_{MP}(D_{eq}) = \text{const} \exp\{-3.67D_{eq}/D_0\} \quad (12)$$

where D_0 is the median volume diameter. This results in an impinging mass distribution of

$$\phi_{MP}(D_{eq}) = \text{const} D_{eq}^3 \exp\{-3.67D_{eq}/D_0\} \quad (13)$$

Figure 9 shows an example of the Marshall-Palmer distribution function and the impinging mass flux distribution function for a typical rain case of $D_0 = 1$ mm. Again it is clear that although there are a significant number of small drops in the ambient distribution, the real icing threat arises from the larger drops in the tail of the distribution.

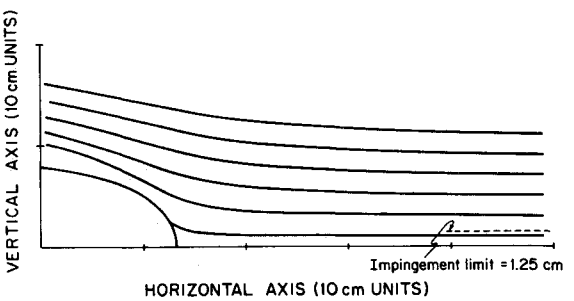

Fig. 6 Droplet trajectories near a half-body.

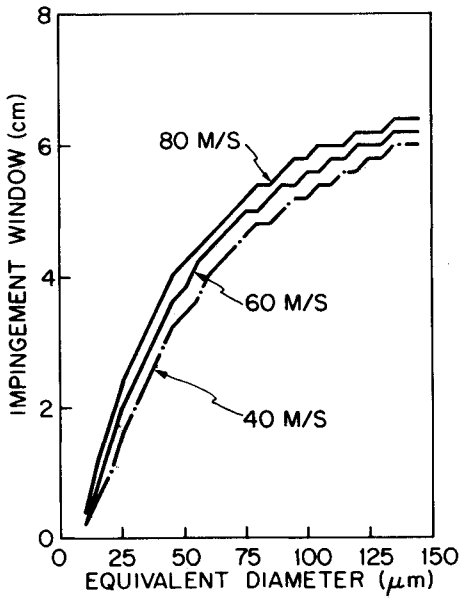

Fig. 7 Impingement window vs equivalent diameter.

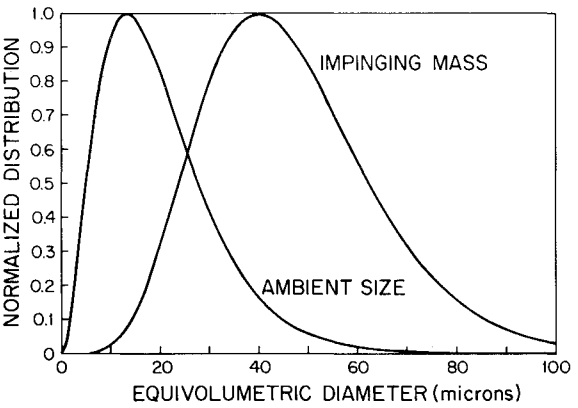

Fig. 8 Khrgian-Mazan ambient cloud droplet size distribution and the resulting impinging mass flux distribution.

Icing Envelopes

The impinging mass approach can be used to determine the relative icing rates that would result from various icing envelopes used for aircraft certification. The intermittent maximum icing conditions from FAR Part 25[9] are shown in Fig. 10. The maximum liquid water content is plotted against median volume diameter for several temperature ranges. Since the liquid water content includes the mass of the droplets, the

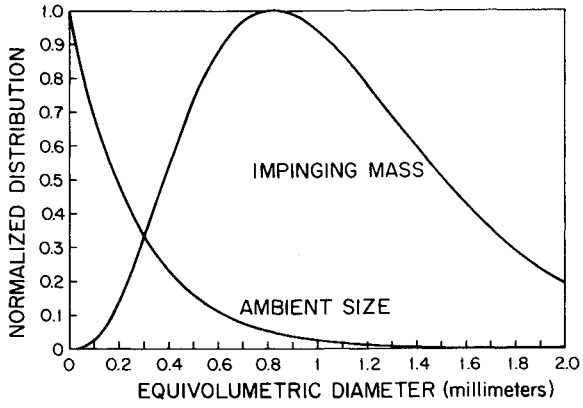

Fig. 9 Marshall-Palmer ambient rain droplet size distribution and the resulting impinging mass flux distribution.

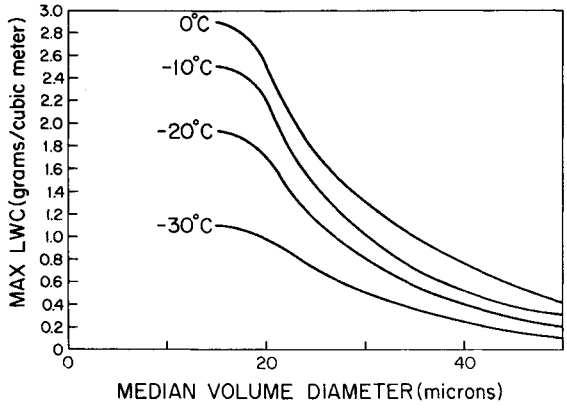

Fig. 10 Intermittent maximum icing conditions from FAR Part 25, App. C.

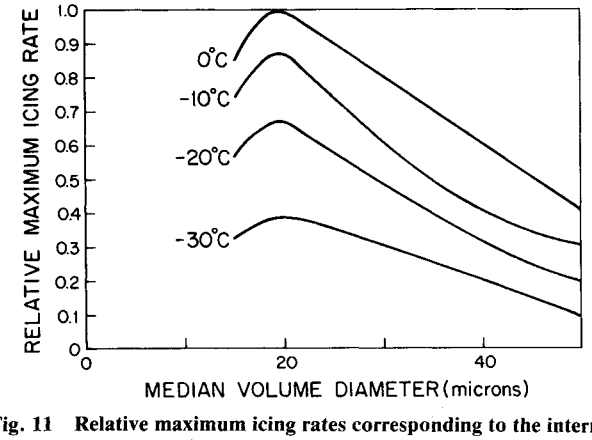

Fig. 11 Relative maximum icing rates corresponding to the intermittent maximum conditions of FAR Part 25, App. C.

relative icing rate can, to first order, be found by simply weighting the LWC by the droplet collection efficiency of the airfoil. The relative maximum icing rates corresponding to the intermittent maximum conditions of FAR Part 25 are shown in Fig. 11. In this case the collection efficiency is assumed to be linear and the icing rate is normalized to the maximum 0°C value. There is a peak in the relative icing rate for all temperatures at approximately 20 μm, and there is still a significant icing rate at the maximum envelope diameter of 50 μm. The maximum relative icing rate decreases with temperature for all sizes.

Recently a more realistic characterization of supercooled clouds below 10,000 ft has been made by Masters[10] and is

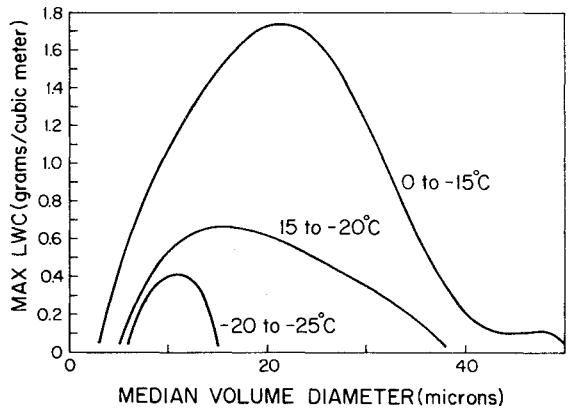

Fig. 12 Characterization of supercooled clouds below 10,000 ft.

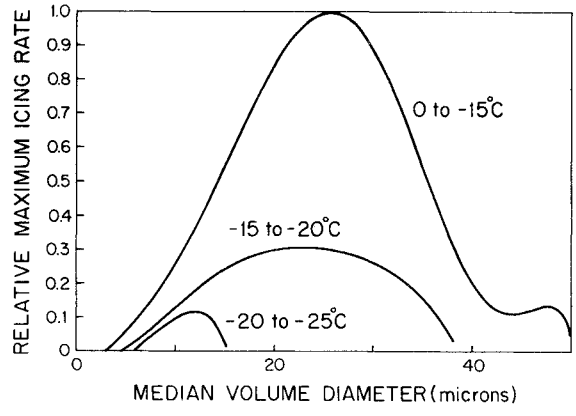

Fig. 13 Relative maximum icing rates corresponding to the characterization of supercooled clouds below 10,000 ft.

shown in Fig. 12. The relative maximum icing rates corresponding to this characterization are shown in Fig. 13, given the previous assumption of a linear collection efficiency. The warm temperature envelope (0 to -15°C) exhibits significantly higher maximum icing rates than the colder envelopes due to the high LWC's and droplet sizes. The -15 to -20°C range has a peak icing rate of 30% of the highest warm value, while the colder range (-20 to -25°C) has a peak value of only 12%.

Conclusion

The results of this work indicate that, for cloud size droplets, the droplet size distribution function is a very important factor in aircraft icing. Larger droplets are seen to present a significantly greater threat than small droplets. For precipitation size droplets the collection efficiency is approximately unity. The implication of the preceding is that even a small liquid water content may be a significant icing threat if it consists of large drops.

The analysis of icing certification envelopes indicates that the 0°C envelopes (which characteristically produce glaze ice) exhibit the highest maximum icing rates due to high liquid water content and large droplet size. Therefore, the 0°C envelopes normally should be the primary focus of icing certification efforts.

The standard droplet drag coefficients of Langmuir and Blodgett[7] commonly used in droplet trajectory codes were found to be inadequate for large droplet sizes due to droplet flattening. A set of empirically modified drag coefficients was generated from well-accepted droplet terminal fall velocity data. A simple two-dimensional code using these coefficients was photographically verified in wind tunnel tests.

Acknowledgments

This work was supported by the National Aeronautics and Space Administration and the Federal Aviation Administration under Grants NAG-1-100 and NGL-22-009-640.

References

[1]Reinmann, J. J., "Selected Bibliography of NACA-NASA Aircraft Icing Publications," NASA TM-81651, 1981.

[2]Bowden, D. T., Gensemer, A. E., and Skeen, C. A., "Engineering Summary of Airframe Icing Technical Data," Federal Aviation Administration, Washington, D. C., FAA-ADS-4, 1963.

[3]Reinmann, J. J., Shaw, R. J., and Olsen, W. A., "NASA Lewis Research Center's Program on Icing Research," NASA TM-83031, 1983.

[4]Norment, H. G., "Calculation of Water Drop Trajectories to and about Arbitrary Three-Dimensional Bodies in Potential Airflow," NASA CR-3291, 1980.

[5]MacArthur, C. D., Keller, J. L., and Luers, J.L., "Mathematical Modeling of Ice Accretion on Airfoils," AIAA Paper 82-0284, Jan. 1982.

[6]Bragg, M. B., Gregorek, G. M., and Shaw, R. J., "An Analytical Approach to Airfoil Icing," AIAA Paper 81-0403, Jan. 1981.

[7]Langmuir, I. and Blodgett, K. B., "A Mathematical Investigation of Water Droplet Trajectories," USAAF TR-5418, 1946.

[8]Gunn, R. and Kinzer, G. D., "The Terminal Velocity of Fall for Water Droplets in Stagnant Air," *Journal of Meteorology*, Vol. 6, Aug. 1949, pp. 243-248.

[9]Federal Aviation Regulation, Pt. 25, App. C, 1974.

[10]Masters, C. O., "A New Characterization of Supercooled Clouds Below 10,000 Feet AGL," Federal Aviation Administration, Washington, D. C., DOT/FAA/CT-83/22, 1983.

[11]Brun, R., Serafini, J., and Gallagher, H., "Impingement of Cloud Droplets on Aerodynamic Bodies as Affected by Compressibility of Air Flow Around the Body," NACA TN 2903, 1953.

[12]Brun, R. and Mergler, H., "Impingement of Water Droplets on a Cylinder in an Incompressible Flow Field and Evaluation of the Rotating Multicylinder Method for Measurement of Droplet-Size Distribution, Volume-Median Diameter, and Liquid-Water Content in Clouds," NACA TN 2904, 1953.

[13]Brun, R., Gallagher, H., and Voyt, D., "Impingement of Water Droplets on NACA 65_1-208 and 65_1-212 Airfoils at 4° Angle of Attack," NACA TN 2952, 1953.

[14]Bergeron, N., "A Method for Numerically Calculating the Area and Distribution of Water Impingement on the Leading Edge of an Airfoil in Cloud," NACA TN 1397, 1947.

[15]Pruppacher, N. R. and Klett, J. D., *Microphysics of Clouds and Precipitation*, 1st ed., D. Reidel Publishing Co., Dordrecht, the Netherlands, 1970.

[16]Marshall, J. S. and Palmer, W. M., "The Distribution of raindrops with Size," *Journal of Meteorology*, Vol. 5, Aug. 1948, pp. 165-166.

[17]Atlas, D., "Advances in Radar Meteorology," *Advances in Geophysics*, Vol. 10, Academic Press, New York, pp. 318-478.